

What *is* Liquid ? [in two dimensions]

Karl Patrick Travis

Department of Materials Science & Engineering

The University of Sheffield

Sheffield S1 3JD, United Kingdom, and

William Graham Hoover with Carol Griswold Hoover

Ruby Valley Research Institute

Highway Contract 60, Box 601

Ruby Valley, Nevada 89833, and

Amanda Bailey Hass

Department of Applied Maths

University of Leeds

Leeds LS2 9JT, United Kingdom

(Dated: December 29, 2021)

Abstract

We consider the practicalities of defining, simulating, and characterizing “Liquids” from a pedagogical standpoint based on atomistic computer simulations. For simplicity and clarity we study two-dimensional systems throughout. In addition to the infinite-ranged Lennard-Jones 12/6 potential we consider two shorter-ranged families of pair potentials. At zero pressure one of them includes just nearest neighbors. The other longer-ranged family includes twelve additional neighbors. We find that these further neighbors can help stabilize the liquid phase.

What about liquids? To implement Wikipedia’s definition of liquids as conforming to their container we begin by formulating and imposing smooth-container boundary conditions. To encourage conformation further we add a vertical gravitational field. Gravity helps stabilize the relatively vague liquid-gas interface. Gravity reduces the messiness associated with the curiously-named “spinodal” (tensile) portion of the phase diagram. Our simulations are mainly isothermal. We control the kinetic temperature with Nosé-Hoover thermostating, extracting or injecting heat so as to impose a mean kinetic temperature over time. Our simulations stabilizing density gradients and the temperature provide critical-point estimates fully consistent with previous efforts from free energy and Gibbs ensemble simulations. This agreement validates our approach.

Keywords: Liquids, Statistical Physics, Molecular Dynamics, Tension, Spinodals, Phase Equilibria

I. WHAT IS LIQUID [IN TWO DIMENSIONS] ?

This work had its origin in the recent death of our colleague Douglas Henderson¹. Bill’s friendship with Doug dated back to the 1960s, their early years as scientists, working at the Lawrence Livermore Radiation Laboratory (Bill) and IBM’s Almaden Research Centre in San José (Doug). Bill and Carol visited Doug and RoseMarie’s homes south of San Francisco and, after the Loma Prieta earthquake of 17 October 1989, in Sandy Utah. These visits became more frequent following the Hoovers’ move to Ruby Valley Nevada in 2005.

All four of us authors have carried out research work devoted to a longstanding challenge of equilibrium statistical mechanics, a better understanding of liquid state structure. The Mayers’ virial series for gases and the Einstein and Debye models for ordered solids provide a relatively accurate understanding of matter’s simplest pair of phases. Liquids remain more mysterious. The question asked by Doug and John Barker in 1976² was a good one and remains so today. Bill adopted this same title as the basis for two publications, one in 1998³, the second in 2014⁴, the latter as part of the celebration of Doug’s 80th birthday.

II. VAN DER WAALS’ 1873 MODEL FOR GASES AND LIQUIDS

Though atomistic liquid structure remains mysterious, van der Waals provided us with his Nobel Prize winning macroscopic “equation of state”. This thermodynamic model describes both gases and liquids as well as the “critical” condition at which the two become indistinguishable. van der Waals chose two material properties to describe the strengths of the attractive and repulsive contributions to the pressure and energy of fluids, both gaseous and liquid. For simplicity we adopt “reduced units” here, setting van der Waals’ material properties a , characterizing attraction, and b , characterizing repulsion, both equal to unity. Throughout this work we use reduced units, setting particle masses and Boltzmann’s constant both equal to unity in addition to the potential parameters and van der Waals’ a and b . In two space dimensions, with kinetic energy $K = \sum(p_x^2 + p_y^2)/2 = NT$, van der Waals’ mechanical and thermal equations of state are:

$$(P + \rho^2)(1 - \rho) = \rho T \text{ [Mechanical] } ; e = T - \rho \text{ [Thermal] } .$$

P , ρ , T , and e — pressure, density, temperature, and internal energy — are the macroscopic thermodynamic variables linked together by van der Waals in his 1873 dissertation on *The*

Continuity of the Gas and Liquid States. For consistency with thermodynamics the resulting mechanical and thermal properties of these fluids are correlated by the second-derivative “Maxwell relation” that follows from the mixed partial derivatives of $[A/T]$ with respect to volume and temperature, $(\partial^2[A/T]/\partial V\partial T) = (\partial^2[A/T]/\partial T\partial V)$ where A is Helmholtz’ free energy, $E - TS$ and S is entropy:

$$(\partial[P/T]/\partial T)_v = (\partial[e/T^2]/\partial v)_T = (\rho/T)^2 \text{ for van der Waals .}$$

According to van der Waals’ model and likewise in accord with nature, the gas and liquid phases can only be distinguished at temperatures below a critical isotherm, on which the unstable minima and maxima of van der Waals’ pressure equation, a cubic in the density, coalesce. The “critical point” on this isotherm is the only location in the pressure-density plane where the isothermal slope and curvature simultaneously vanish:

$$(\partial P/\partial \rho)_T = 0 \text{ and } (\partial^2 P/\partial \rho^2)_T = 0 \longrightarrow \{ P_c = 1/27, \rho_c = 1/3, T_c = 8/27 \} .$$

At this critical point the two fluid states, gas and liquid, become indistinguishable. They also become hard to investigate as the vanishing first derivative implies infinite compressibility, $-d \ln V/dP$, and zero sound speed, as $c = \sqrt{(\partial P/\partial \rho)_S} \propto \sqrt{(\partial P/\partial \rho)_T}$, where S is entropy. This singular behavior of the pressure derivatives is reflected in the macroscopic nature of critical density fluctuations big enough to see. The fluctuations are observed visually as a milky “critical opalescence”.

For any temperature less than the critical temperature value $T_c = (8/27)$ van der Waals’ model gives two values of the density which can coexist at mechanical and thermal equilibrium. In addition to these “binodal” points there are two other density values on every subcritical isotherm and on some adiabats between which the van der Waals equation of state is mechanically unstable. These pairs of points form the high-density and low-density boundaries of unstable isothermal and adiabatic “spinodal regions”, within which at least one of the two van der Waals’ compressibilities is negative. Straightforward algebra shows that van der Waals’ adiabatic spinodal line [where $(\partial P/\partial \rho)_S$ vanishes] has the same form as the isothermal line, but at half the temperature :

$$T_{\text{isothermal}} = 2\rho(1 - \rho)^2 = 2T_{\text{adiabatic}} .$$

The van der Waals model’s “binodal” equilibrium coexistence curves and the “spinodal” curves of divergent compressibility are characteristic of many real macroscopic fluids and

common microscopic fluid models which include both attractive and repulsive pair forces. The best known microscopic model is Lennard-Jones' 12/6 potential from the 1920s:

$$\phi_{LJ}(r) = (1/r)^{12} - 2(1/r)^6 \longrightarrow \phi'(1) = 0 ; \phi(1) = -1 .$$

The van der Waals and Lennard-Jones phase diagrams are compared in **Figure 1**. Although van der Waals' equation has no solid phase, a more sophisticated state-equation model, based on the known hard-disk equation of state, for disks of diameter σ and number density $\rho = (N/V)$:

$$(PV/NkT) = (PV/NkT)_{\text{disks}} - \rho \text{ [with } B_2 = (\pi/2) \text{ and diameter } \sigma \equiv 1 \text{ for disks] ,}$$

provides a three-phase equation of state analogous to van der Waals' two-state solution. The critical parameters depend upon the reduced units chosen for the hard-disk model. With disk diameter σ and Boltzmann's constant set equal to unity this model gives $(P_c, \rho_c, T_c) = (0.019, 0.269, 0.216)$ with a dimensionless compressibility factor $(PV/NkT) = 0.326$, quite close to the value of $(1/3)$ obtained by using a maximally truncated three-term virial expansion, $(PV/NkT) = 1 + B_2\rho + B_3\rho^2$.

It is evident from **Figure 1** that pair potential models can provide a semi-quantitative understanding of the coexistence and coalescence of the less-dense gas and more-dense liquid phases of simple fluids, where both phases are formed from the same ingredients.

Understanding the details of the microscopic structure leading to this macroscopic behavior is an excellent illustration of the problem areas all four of us authors have enjoyed exploring. Before entering into the details of our own work let us consider the progressive steps leading from van der Waals equation in the late 1800s up to Barker and Henderson's review a century later.

III. THEORIES AND MODELS OF THE LIQUID STATE

In the late nineteenth century critical-point experiments were carried out by heating a known quantity of liquid in a sealed tube with an obvious "meniscus". That word, "meniscus", comes from the Greek for "curved moon". It is because the two phases interact with their container's surface differently that the meniscus separating them is curved. Near the "critical point", where gas and liquid become indistinguishable, dramatic density fluctuations broaden and destroy the meniscus separating the two coexisting phases.

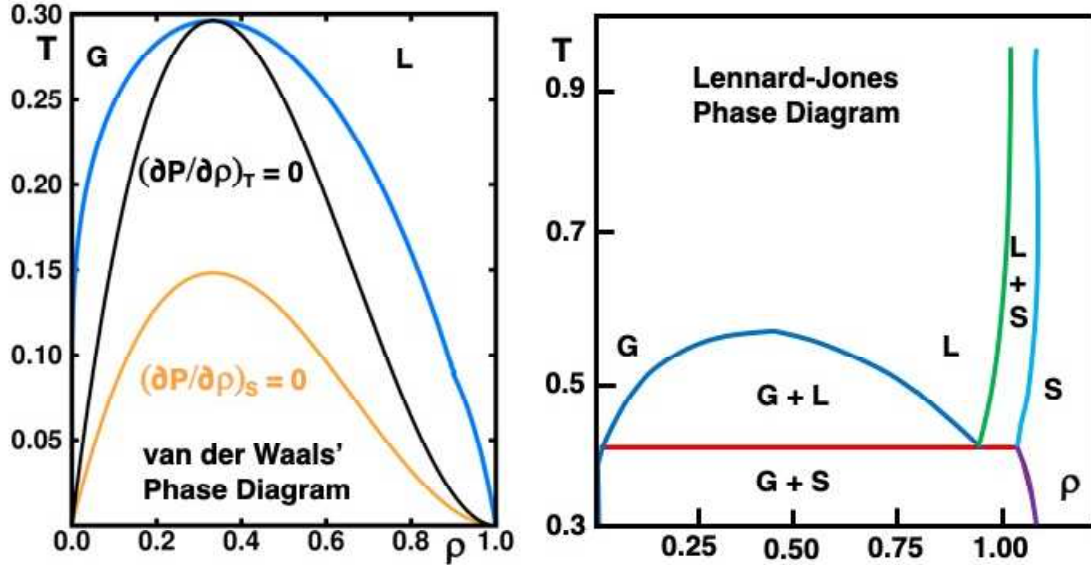


FIG. 1: At the left is van der Waals' phase diagram and at the right the two-dimensional Lennard-Jones analog⁵. In the van der Waals case the isothermal and isentropic spinodal lines, where the corresponding compressibility diverges, are shown. In the Lennard-Jones case, with its solid phase, there is a triple point near $T = 0.4$ below which the gas and solid coexist. Between the triple-point temperature and the critical temperature (roughly 0.56) lower-density gas and higher-density liquid can coexist.

In 1882 Hannay declared “The formation of a meniscus is the only test of the liquid state”⁶. That meniscus definition is superior to Wikipedia’s notion, “Liquid is a nearly incompressible fluid that conforms to the shape of its container”. Hannay was right. A liquid-gas interface, or meniscus, with the liquid the denser of the two fluid phases, is necessary to distinguish the one phase from the other. Wikipedia’s liquid definition would include dense fluids of hard disks or spheres. But neither of those hard-particle systems has the attractive forces necessary to stabilize a liquid phase.

By 1900, with the advent of Boltzmann and Gibbs’ statistical mechanics, atomistic models became important. Kinetic theory and lattice dynamics offered useful descriptions of gases and solids. Good structural models for liquids were absent. This lack soon motivated the construction of physical models of liquid structure. In 1930s London John Bernal simply added more and more ball-bearing particles to ball-and-stick or conglomerate balls-in-paint structures. Bernal found that the radial distributions of pairs of balls resembled those inferred from radiation experiments on real liquids. At about this same time Joel Hildebrand,

in Berkeley, immersed more than 100 gelatin balls in a fish tank, likewise finding that the distribution of the balls' separations resembled the distributions of interparticle distances in liquid argon, scaled up by eight-or-so orders of magnitude. Bernal and Hildebrand were looking for bulk liquid structure, not the interfacial menisci stressed by Hannay.

John Barker devoted most of his working life to the understanding of liquids⁷, publishing his only book, *Lattice Theories of the Liquid State* in 1963, just as it was becoming clear that lattices were not a proper starting point for “understanding”. Before he and Doug Henderson had discovered and implemented perturbation theory Barker had attempted to improve his understanding of liquids by extending “lattice theories”, like the Ising Model. That model, with its hole-particle symmetry, seems very distant to real liquids. Barker invented “tunnel models”, taking advantage of the mathematical simplicity of one-dimensional chains of particles, coupled with a symmetry-breaking description of the tunnel locations. In tunnel models for simple atoms one-third of the degrees of freedom are longitudinal and two-thirds are transverse to the tunnels. Barker’s collaboration with Doug in the 1960s, based on a perturbation theory of the Helmholtz free energy, was soon to provide a surprisingly useful predictive theory. The theory provided all the liquid thermodynamic properties based on known properties of hard spheres. This hard-sphere-based theory’s success seems a bit puzzling because the underlying model is itself incapable of providing the two-fluid meniscus characteristic of real liquid-gas coexistence.

IV. PROGRESS IN UNDERSTANDING FROM COMPUTER SIMULATIONS

Soon after World War II, in the 1950s, the advent of computers opened up completely new research opportunities. Alder, Jacobson, Wainwright, and Wood developed Monte Carlo and molecular dynamics simulation algorithms modeling equilibrium distributions of dozens or hundreds of hard particles in two and three space dimensions. They discovered and characterized the hard-disk and hard-sphere fluid-solid transitions^{8,9}. These melting-freezing transitions occur when the solid phases are expanded about ten percent in (x, y) or (x, y, z) , corresponding to melting densities, relative to close-packed, of about $(4/5)$ (for disks) and $(3/4)$ (for spheres).

In 1958 Jerry Percus and George Yevick formulated an integral equation for the pair distribution function¹⁰. Mike Wertheim solved the equation analytically for hard spheres

five years later¹¹. A numerical solution of the hard-disk analog appeared half a century later, in 2008. The analytic work for spheres gave an excellent approximation to the hard-sphere distributions from Monte Carlo and molecular dynamics simulations. These developments led to the successful refinements of perturbation theory reviewed by Barker and Henderson in 1976. Their approach was paralleled by several other dedicated scientists, among them Farid Abraham, Hans Andersen, Frank Canfield, David Chandler, Ali Mansoori, Jay Rasaiah, George Stell, and John Weeks.

V. BARKER AND HENDERSON'S DESCRIPTION OF "LIQUIDS"

After a decade working together Barker and Henderson addressed our title question from the standpoint of perturbation theory, in 1976. Rather than constructing physical many-body models they adopted the results of hard-particle computer simulations to develop and evaluate a perturbation theory based on the Percus-Yevick hard-sphere distribution function. They treated attractive forces as a perturbation added to a reference repulsive potential. The resulting free energy calculations related the thermodynamics of homogeneous liquids to hard-sphere fluid-phase properties. Helmholtz' and Gibbs' free energies can alternatively be found by integrating equation of state data taken from Monte Carlo or molecular dynamics simulations. With today's computers brute-force simulation is the more practical and much-simpler approach.

Barker and Henderson summarized the state of the art of the 1970s perturbation work in their review. In its simplest form liquid perturbation theory is based on optimizing a reference-system's hard core size by minimizing Helmholtz' free energy at fixed values of the density and temperature. The success of this theory is due to the fact that thermodynamics requires no treatment of mixed-phase systems. Consequently perturbation theory can be based on reference hard-particle systems which lack a liquid phase and its corresponding meniscus. Bill Wood, at Los Alamos, pointed out that the hard-particle systems' fluid-solid surface tension is negative. Thus drops of hard disks and spheres don't form. Unlike models with attractive forces hard particles don't form clusters.

VI. CONCEPTUAL DIFFICULTIES : LIQUIDS’ “SPINODAL REGION”

There is a tremendous literature on the “spinodal” region of the phase diagram¹²⁻¹⁴. For van der Waals’ equation this is usually taken to be the mechanically-unstable region with negative isothermal compressibility. In principle a negative compressibility, either isothermal or adiabatic, generates exponential growth of density fluctuations and so is to be prohibited in realistic fluid models. Thus the borders of a spinodal region for real fluids, if there were one, would be hard to access and describe. Wedekind *et alii* described access to the spinodal regions well¹³:

“It would be very complicated, if not practically impossible, to reach the spinodal.”

The internet reveals that “spinodal” originated as a synonym for “cusp”. This explanation seems curiously incomplete (and mercifully absent from most textbooks) as no cusp is apparent in realistic phase diagrams like those of van der Waals or the Lennard-Jones potential. See again **Figure 1**. We consider a region with negative compressibility strange, artificial, and “unstable”. Shamsundar and Lienhard explicitly object¹² to the term “unstable”, citing the reality of nearby states of superheated liquids and supercooled gases, likewise nonequilibrium states not appearing in a conventional single-valued phase diagram. Any *fluid* under tension and subject to mechanical noise cannot persist unchanged for long. Solids do characteristically exhibit tensile strength but still can suffer shear instabilities. We will illustrate such models later in this work. There is as yet no accepted standard for bulk “liquid” structure, though not for lack of trying.

In the context of the usual single-component thermodynamics for a simple material like argon the spinodal region of the phase diagram corresponds, at least conceptually, if not in the laboratory, to a mix of a denser liquid and a less-dense gas. Because such a system isn’t homogeneous it is clear that a simple phase diagram or a model like van der Waals’ is an incomplete description. Simulations in this region lead to highly-complex evolving structures of transient rotating clusters or clumps of particles. The properties of nonequilibrium clusters are complex, involving surface tension and rotational contributions to the energy, making the characterization of “pressure” somewhat uncertain.

In our own effort to clarify the ambiguities of “spinodal states” for two-dimensional

fluids we thought it prudent to consider three different initial conditions, all of them equally plausible *a priori*. With Lennard-Jones forces both the square lattice, sufficiently expanded to reach a density of 0.4, or a triangular lattice expanded to that same density, have energies exceeding that at the critical point and so cannot serve as models for a spinodal state using conservative mechanics. A simple way out of this energy problem is to consider *isothermal* molecular dynamics, starting and finishing at an imposed kinetic temperature less than critical and greater than that at the triple point. Such a choice lies somewhere in a nonequilibrium liquid range. In two space dimensions, the Lennard-Jones critical and triple-point temperatures are on the order of 0.56 and 0.4 according to Barker, Henderson, and Abraham⁵. We have chosen the temperature 0.5 as our standard initial (and final, time-averaged) condition for our exploratory molecular dynamics simulations. See **Figure 2** for a sample evolution from an unstable square lattice. An expanded triangular lattice provides a similar history. A third possibility, illustrated in **Figure 3** is to divide up the system into cells with the structure in each cell chosen randomly. A special case of this choice takes a regular stress-free lattice with the number of randomly-located vacancies chosen to satisfy the desired density, 0.4 in our case, close to the Barker-Henderson-Abraham estimate of the critical density in **Figure 1**.

The two sample evolutions shown here are typical of the spinodal region. The equilibrium phase diagram disallows states under tension. There is an initial exponential growth of density fluctuations, followed by a slower coarsening of clusters to form a percolating cluster spanning the entire volume¹⁴. The details of the first exponentially unstable phase depend upon the initial conditions. The details of the second phase, with the nonequilibrium equilibration of growing clusters, are relatively easy to see but hard to predict¹⁵, suggesting the exploration of alternative methods for characterizing liquids.

Gravity can take us in the direction of Hannay’s meniscus. The evolution of an initial state toward the formation of a meniscus can be visualized by adding a small gravitational field to the dynamics. With a field the liquid state lies below the vapour with which it equilibrates. The **Figure 1** phase diagram for Lennard-Jones’ potential indicates that a liquid about six times denser than its vapour should be stable at a temperature of 0.5, well below the critical temperature of 0.56 and above the triple point temperature of 0.4. This suggests a feedback dynamics similar to the “Gibbs ensemble” algorithm, with particles transferred from interacting simulations with a common pressure and temperature. Feedback within a

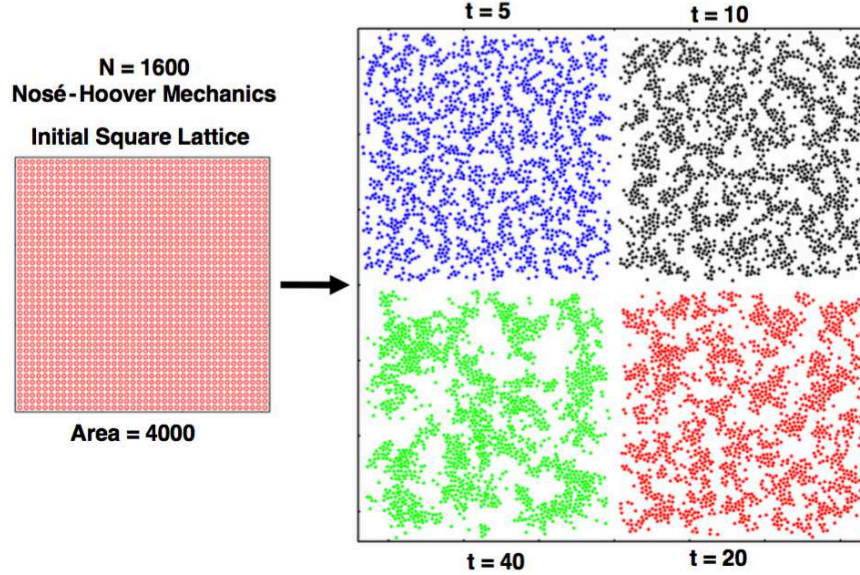


FIG. 2: Four snapshots in a “spinodal” evolution. The dynamics is Nosé-Hoover isothermal at the subcritical temperature $T = 0.5$. The initial condition, at the left, is a perfect square lattice of area 4000 containing 1600 Lennard-Jones particles. Fourth-order Runge-Kutta integration with $dt = 0.005$ to time 40. The instability of the lattice gives rise to coarsening, soon forming a percolating cluster spanning the volume¹⁴. Boundary potentials quartic in dx and dy repel any particles with $|x|$ or $|y|$ exceeding $\sqrt{1000} = 31.623$.

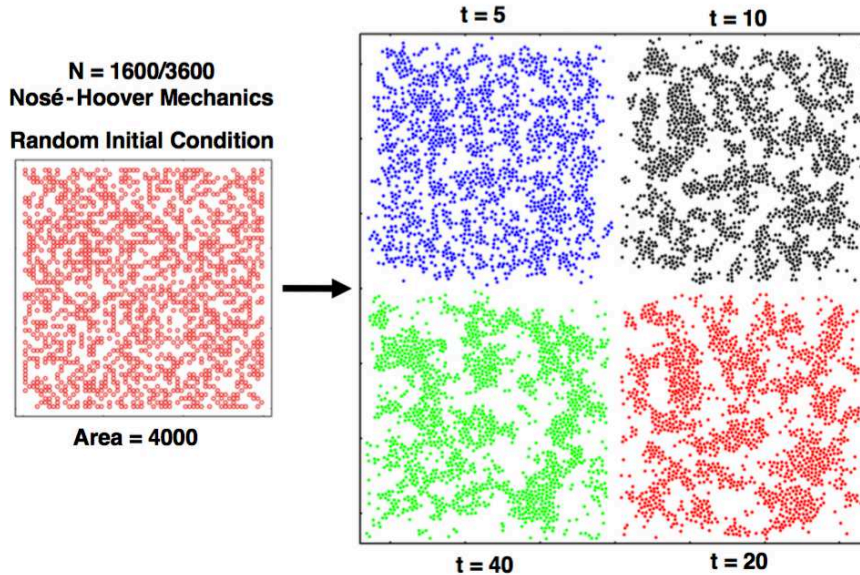


FIG. 3: Four snapshots in a “spinodal” evolution. The dynamics is Nosé-Hoover isothermal at the subcritical temperature $T = 0.5$. The initial condition was a perfect square lattice of 3600 sites in an area 4000 with 1600 of the sites, randomly chosen, containing Lennard-Jones particles. Boundary potentials quartic in dx and dy repel any particles with $|x|$ or $|y|$ exceeding $\sqrt{(1000)} = 31.623$.

single simulation provides a less singular evolution. Let us turn to dynamics in the presence of an external gravitational field.

VII. IMPLEMENTING A “LIQUID” VISION WITH MOLECULAR DYNAMICS

In the present work we consider the need, and fill it, for a “meniscus” separating a “gas” from a “liquid” fluid. We stabilize and investigate the interfaces defining phase boundaries. To do this we first of all model the idea of a physical “container”, to which all the particles in our simulations must conform. To simulate the dynamics of such a manybody system we enclose it within a special fixed boundary, a smooth nearly-rigid container modeled with a quartic repulsive surface potential.

In keeping with the expected accuracy of a fourth-order Runge-Kutta integration of the motion equations we adopted one-sided quartic potentials to contain our simulations. We begin with both rectangular and circular “containers” for our molecular dynamics. The boundary potential energy in the circular case is $(dr^4/4)$ where dr is the depth of penetration beyond a circular boundary of radius r . To reflect escaping particles in the rectangular case the boundary potentials are $(dx^4/4)$ and $(dy^4/4)$ imposed on the four sides of a rectangular container. dx and dy are the penetrations beyond the vertical and horizontal walls of a rectangular container. See **Figures 4 and 5** for typical equilibrium snapshots of 400 Lennard-Jones particles with the density and kinetic temperature at a fluid state point well above the gas-liquid coexistence curve, $\rho = 0.4$; $T = 1 > T_C \simeq 0.56$. The wild density fluctuations seen in these two equilibrium snapshots rightly suggest that time-averaging is needed to aid the analysis of the gas-liquid meniscus structure.

The figures document that typical penetrations, beyond the quartic boundaries, are about one particle diameter, consistent with an energy-based estimate :

$$(dx^4/4) \simeq (dy^4/4) \simeq (dr^4/4) \simeq T = 1 \rightarrow dr \simeq 1.414 .$$

With these straightforward model boundary potentials providing a conforming container we next seek out a means for emphasizing and localizing the meniscus characteristic of the liquid state.

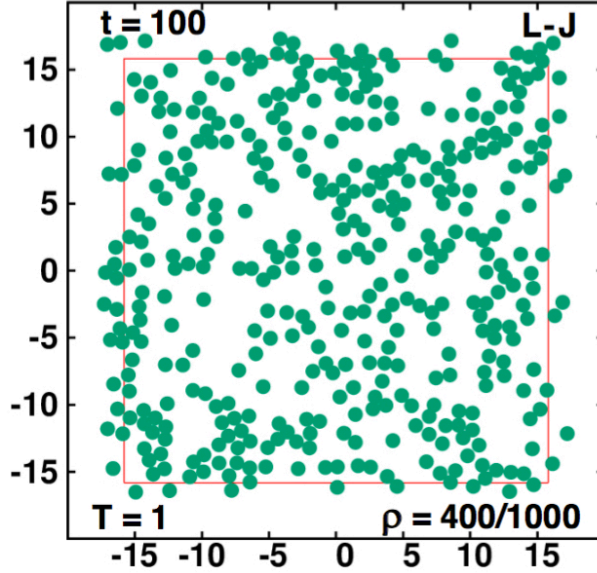


FIG. 4: An equilibrium snapshot of 400 Lennard-Jones particles at $T = 1$ confined by square boundary potentials at $\pm\sqrt{250} = 15.811$. The density is 0.4. The simulation time $t = 100$ is adequate for equilibration. Here, and mostly throughout, we use fourth-order Runge-Kutta integration with a timestep $dt = 0.005$.

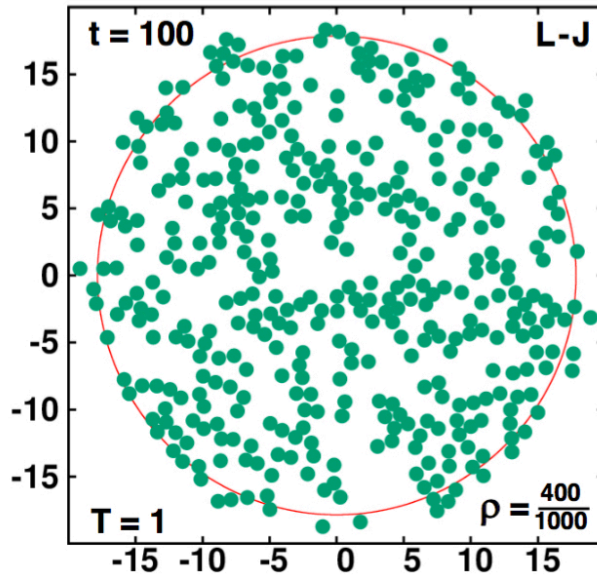


FIG. 5: An equilibrium snapshot of 400 Lennard-Jones particles at $T = 1$ confined by a circular quartic boundary potential at $r = \sqrt{1000/\pi} = 17.841$. The snapshot was taken after 20,000 timesteps with $dt = 0.005$. The density is 0.4. The simulation time $t = 100$ is adequate for equilibration.

VIII. STABILIZING THE MENISCUS WITH GRAVITY

Barker and Henderson were satisfied with a formal semiquantitative perturbation theory based on a reference hard-core potential. We prefer a more physical approach, based on observations of phase equilibria. For us, a stable interface separating a liquid from its less-dense gas is the necessary and defining aspect of liquid behavior. From the observational standpoint to be sure one is viewing a liquid (as opposed to a gas or hard-particle fluid) requires observing the interface separating the two varieties of simple fluids, the liquid and the gas. This is easy to do by simulating a gas bubble surrounded by liquid or a liquid drop in a dilute gas; but such clearcut observations become blurred nearer the “critical point” where fluctuations are macroscopic. There the manybody dynamics is dominated by percolating clusters of macroscopic size.

To encourage our particles’ conformation to their container with a visible meniscus we include a second innovation, a constant vertical acceleration, $-g$ for each of our computational particles. This constant downward force is added to the pairwise forces from other particles and to the boundary forces defining our containers :

$$F = F_{pair} + F_{penetration} + F_{gravity} .$$

We harbor the optimistic assumption that such a combination of particle plus boundary plus gravitational forces will accommodate not only a gas-liquid interface but also the liquid-solid one. In 1977 Ladd and Woodcock demonstrated that sufficiently close to the triple point it is possible to see both of these liquid interfaces simultaneously¹⁶. At such a “triple point” there are no thermodynamic “degrees of freedom”. All three phases coexist at the same pressure and temperature. By adding gravity we provide our fluid systems with a pressure gradient satisfying the continuum force balance, $(dP/dy) = -\rho g$ in the stationary state. The pressure gradient (dP/dy) forces the fluid to conform its shape to its container, and, over a wide range of pressures, serves to localize and illustrate the gas-liquid and liquid-solid interfaces.

The phenomena of yield stress (for the solid) and surface tension (for the liquid) could prevent shape conformation unless these properties can be overcome by gravitational or rotational forces. We have chosen gravity as the simpler of these two choices. Finally, in order to prescribe the overall temperature of our two-phase or three-phase systems we apply

Nosé-Hoover isothermal dynamics with a target temperature T_{NH} :

$$T_{NH} = \langle (K/N) \rangle = \langle (p_x^2/2) + (p_y^2/2) \rangle .$$

IX. IMPOSING KINETIC TEMPERATURE ON MOLECULAR DYNAMICS

The fundamental conceptual basis of our present work is conservative Hamiltonian molecular dynamics. We include the forces and potential energies from a constant gravitational field as well as those describing special containerized boundary conditions. For flexible control of the simulations, and to accelerate convergence, we generalize the underlying mechanics to include Nosé-Hoover control of temperature. Let us next outline the Nosé-Hoover control mechanism.

Molecular Dynamics with specified kinetic temperatures has made steady-state nonequilibrium simulations a standard method for simulating steady nonequilibrium flows of mass, momentum, and energy. In 1984 Nosé introduced his novel time-reversible Hamiltonian dynamics. He treated the kinetic temperature as an independent variable imposed on the dynamics. This is accomplished by augmenting the manybody motion equations with a time-reversible friction coefficient ζ . Hoover provided a simplified formulation of Nosé's approach which has been widely adopted. We use it here:

$$\{ \dot{x} = p_x ; \dot{p}_x = F_x - \zeta p_x ; \dot{y} = p_y ; \dot{p}_y = F_y - \zeta p_y \}$$

$$\dot{\zeta}(t) = (1/N\tau^2)[K(t) - \langle K \rangle] [\text{Nosé - Hoover Dynamics}] .$$

Here $\langle K \rangle$ is the constant target value of the kinetic energy, imposed by ζ . In the two-dimensional systems we consider the kinetic temperature is $T = (1/N) \sum (p_x^2 + p_y^2)/2 = (K/N)$, and the relaxation time τ can be chosen as a typical collision time. For the current simulations we have chosen $\tau = 1$.

If it is desirable to accelerate convergence it is quite practical to begin with a higher imposed temperature and/or a higher gravitational field. With Runge-Kutta integration it is perfectly feasible to specify analytic time dependences for these target temperatures and fields, $T(t)$ and $g(t)$, within the equations of motion.

For simplicity and clarity we restrict our investigations to two-dimensional systems. We look directly at coexisting phases, so as to avoid the need for free energy calculations.

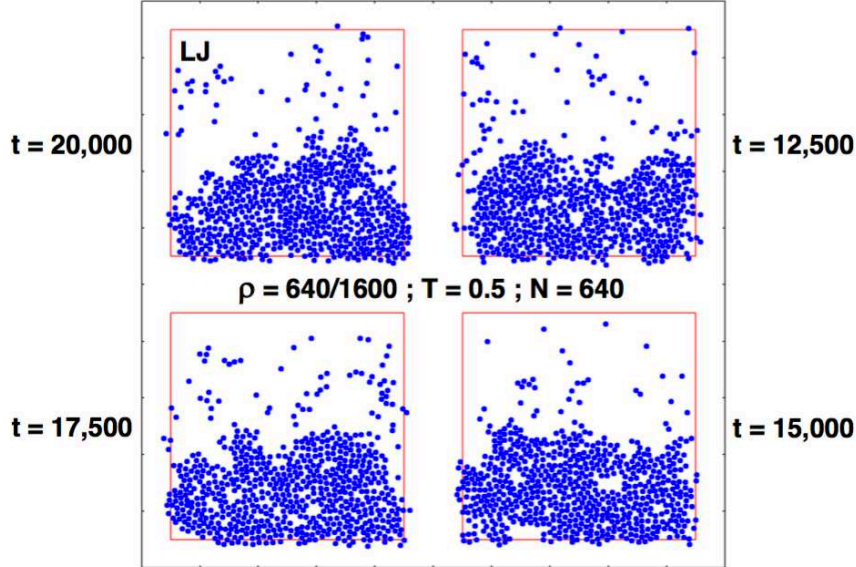


FIG. 6: Four Nosé-Hoover Lennard-Jones snapshots at times 12,500, 15,000, 17,500, and 20,000. Gravitational field 0.01 with 640 particles confined by a square boundary, quartic potentials at $|x| = 20$ and $|y| = 20$. Timestep 0.005 and $T = 0.5$. Fourth-order Runge-Kutta integration.

Corresponding implementations for three-dimensional systems are straightforward. This will be clear as we discuss the necessary diagnostics for analyzing the results of our computer simulations.

X. ISOTHERMAL LENNARD-JONES FLUIDS WITH GRAVITY

The simulations leading to **Figures 4 and 5**, when time-averaged, correspond to equilibrium homogeneous fluids due to the lack of any organizing field. **Figures 6 and 7**, which include gravity, illustrate very different situations incorporating menisci. They snapshot the evolving morphology of 640 Lennard-Jones particles in square and round containers of enclosed volume 1600, corresponding again to a near-critical density $\rho = 0.4$. In both these highly inhomogeneous systems the gravitational field strength is $g = 0.01$. The slightly subcritical kinetic temperature, $\langle (p_x^2 + p_y^2)/2 \rangle$, is 0.5, and the Nosé-Hoover relaxation time imposing it is unity. The underlying two-million-timestep simulations including all $(640 \times 639/2)$ Lennard-Jones interactions take a half day on a desktop computer. The two field-driven figures, with four sample snapshots from the last halves of the runs, both show a denser phase $\rho \simeq 1$ below a lower-density gas phase $\rho \simeq 0.1$. We will see in **Figure 17** that time-averaging isothermal snapshots provides additional simplicity and considerable clarity.

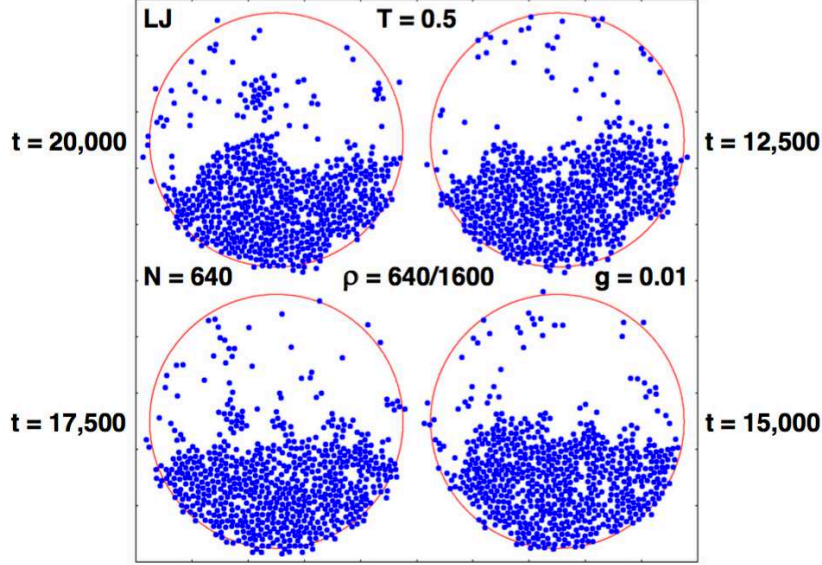


FIG. 7: Four Nosé-Hoover Lennard-Jones snapshots at times 12,500, 15,000, 17,500, and 20,000. Gravitational field 0.01 with 640 particles confined by a circular boundary at $r = \sqrt{x^2 + y^2} = \sqrt{1600/\pi} = 22.568$. Timestep $dt = 0.005$ and $T = 0.5$.

Koch, Desai, and Abraham’s comprehensive spinodal work using the Lennard-Jones potential¹⁴ suggests a gas-liquid density ratio of roughly (1/6) at $T = 0.5$. In our earlier exploratory simulations the gravitational field strength obeyed a feedback differential equation based on generating our desired factor of six in the density difference, $\dot{g} = 0.01[N^{gas}(t) - (N/7)]$. N^{gas} is simply the number of particles with positive y coordinates. Because the resulting fluctuating field strength was close to 0.01 we adopted the simpler and smoother approach of using a constant gravitational field for **Figures 6 and 7**. With cartesian coordinates $\{ q = (x, y), p = (p_x, p_y) \}$ the $4N + 1$ differential equations of motion are:

$$\{ \dot{q} = p ; \dot{p} = F - \zeta p \} ; \dot{\zeta} = (K/N) - 0.5 ; K \equiv \sum (p_x^2 + p_y^2)/2 .$$

The summed forces F on each particle include pair forces, gravity, and the container forces. We add on the thermostat forces, $\{ -\zeta p \}$, assigned the task of imposing isothermal conditions throughout the container. The particle interactions are Lennard-Jones without any cutoff, with quartic boundary potentials on the sides of the square container and along the perimeter of the circular container.

Individual densities $\{ \rho_i \}$, at each particle or at any grid point (x_g, y_g) , can be defined, and evaluated numerically, with the help of Leon Lucy’s two-dimensional “smooth-particle”

weight function¹⁷. The weight function spreads the influence of each particle very smoothly (two continuous derivatives everywhere) in space. For example the “delta-function” density of each two-dimensional particle and of its properties (such as velocity, energy, and pressure tensor) are likewise distributed smoothly within a circle of radius h . The weight function is maximum at the particle’s location and vanishes on and beyond its bounding circle. The corresponding density distribution in the differential neighborhood $rdrd\theta$ of a particle is

$$\rho(r, \theta) = (5/\pi h^2)(1 - 6z^2 + 8z^3 - 3z^4) ; z \equiv r/h .$$

A reasonable choice of the range h of Lucy’s weight function for most atomistic simulations is 2 or 3 particle diameters. We have chosen 2 throughout the present work.

The normalization prefactor in one dimension, $(5/4h)$ for $-h < dx < +h$, is replaced by $(5/\pi h^2)$ for normalization within a circular area with $\pi r^2 < \pi h^2$:

$$\int_0^h 2\pi r dr (5/\pi h^2)(1 - 6z^2 + 8z^3 - 3z^4) \equiv 1 \text{ where again } z \equiv (r/h) .$$

Lucy’s smooth weight function is convenient for comparing the results of atomistic simulations to the predictions of continuum mechanics, as we shall presently demonstrate, when seeking interfaces identifying the liquid phase.

A simple one-dimensional example illustrates the usefulness and power of smooth-particle weighting. Consider the one-dimensional lattice of points at the integers so that the coarse-grained “density of points” is unity. Using Lucy’s smooth-particle weighting function normalized for one-dimensional distributions,

$$w(|dx| < h) = (5/4h)(1 - 6z^2 + 8z^3 - 3z^4) \text{ where } z \equiv |dx|/h ,$$

gives for the density at each integer point 1.0156 for a “smoothing length” $h = 2$ and 1.0031 for smoothing length $h = 3$. The local density in a one-dimensional system at the grid point x_g is the summed-up contribution from nearby particles $\{ x_i \}$ within a distance h of the grid point:

$$\rho(x_g) \equiv \sum_i w(|x_i - x_g|) .$$

Applying this same definition, in between the integers, at the various midpoints $\pm(1/2)$, $\pm(3/2)$, \dots , the smoothed densities are 0.9863 and 0.9973 respectively for smoothing lengths of 2 and 3.

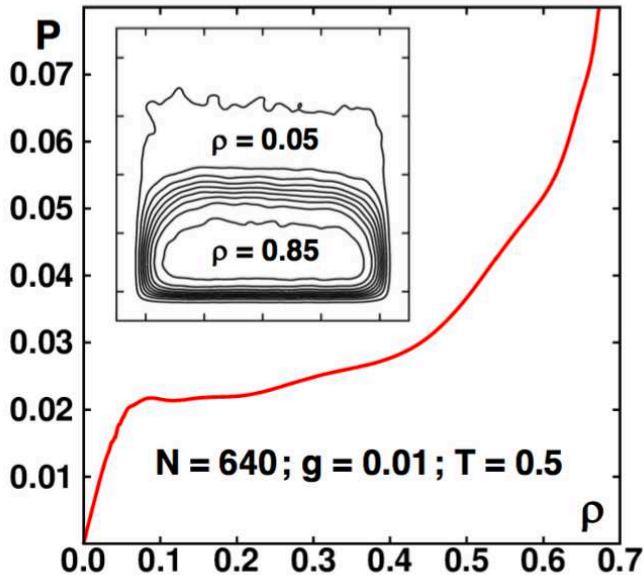


FIG. 8: Time-averaged density contours from 0.05 to 0.85 for 640 Lennard-Jones particles at $T = 0.5$ and overall density 0.4. The quartic square boundaries are located at ± 20 . Space and time averages, over the horizontal x coordinate in space, and using the final two million timesteps in a four million timestep run, in time, provide the $\langle P \rangle(\langle \rho \rangle)$ profile giving the structure of the meniscus perpendicular to that interface.

Likewise, carrying out a one-dimensional average over x for a few hundred horizontal strips the y -dependent pressure and density, $\{ \langle P(y) \rangle \}$, $\{ \langle \rho(y) \rangle \}$ can be computed with one-dimensional weights including all particles within a vertical separation $|dy| < h$ of the gridpoint in question, where h is the range of the Lucy function. The spatial and temporal averaging process involves three distinct steps: [1] Compute individual particle properties such as ρ_i and P_i using two-dimensional smoothing; [2] Convert the particle data into spatial averages for a y grid using one-dimensional smoothing; [3] Combine the spatial values by averaging over as many as millions of timesteps.

Figures 8 and 9 show time-averaged pressure and density profiles for the two boundary conditions, square and circular. In both cases wildly fluctuating snapshot configurations, time-averaged over the last half of a two-million timestep simulation, provide a smooth meniscus with a width of just a few particle diameters. The pressure and density, averaged over both time and x indicate a horizontal isotherm rather than a van der Waals' loop.

Figure 10 compares the structures of the meniscus, pressure versus density, for a series of five values of the gravitational field from 0.01 to 0.05. The upper segment of each of

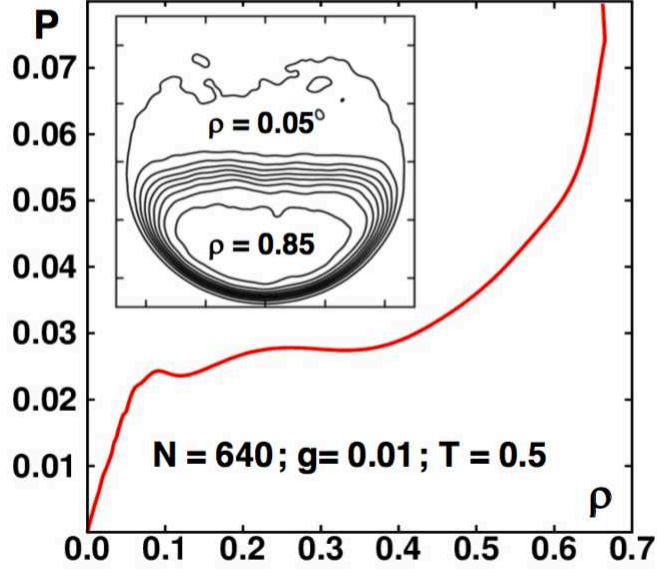


FIG. 9: Time-averaged density contours from 0.05 to 0.85 for 640 Lennard-Jones particles at $T = 0.5$ with overall density 0.4. The circular boundary potential begins at $r = \sqrt{(1600/\pi)} = 22.568$. Averages over the horizontal x coordinate using two million timesteps provide the $\langle P \rangle(\langle \rho \rangle)$ profile giving the structure of the meniscus.

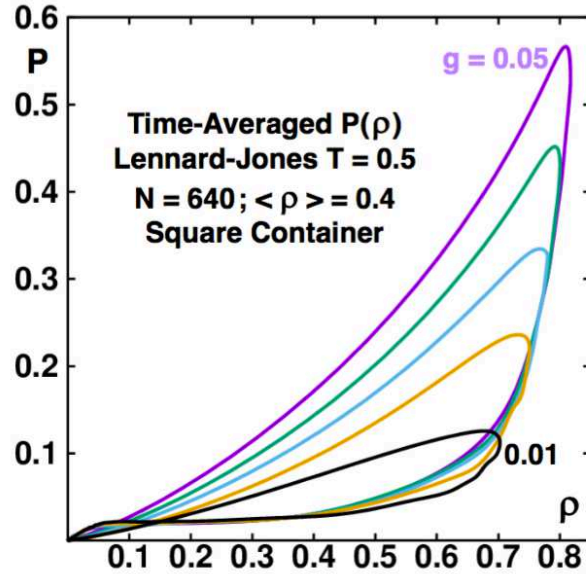


FIG. 10: Time-averaged pressure as a function of time-averaged density using the last half of two million Runge-Kutta timesteps for 640 Lennard-Jones particles in a 40×40 quartic box. Five separate curves are shown corresponding to field strengths 0.01, 0.02, 0.03, 0.04, and 0.05. The lower portions of the five curves correspond to the meniscus separating liquid from gas. The good agreement indicates very little dependence of the pressure-density correlation upon field strength. The simulation with $g = 0.01$ used the last half of a four-million-timestep run.

the five traces corresponds to the high-density high-pressure region near the bottom of the container, which supports the entire weight of the 640 Lennard-Jones particles. The low-density low-pressure region near the bottom of the plot (where the five traces agree) describes the meniscus atop most of the fluid. The good agreement of all five indicates that the present introduction of gravity into critical-region simulations provides accurate unambiguous estimates of the subcritical isotherms without the need for free energies or a Maxwell construction. Contour plots, as in **Figures 8 and 9** are probably the best diagnostic tool for the meniscus as the density near the centre of the container can be assessed and, when time-averaged, is guaranteed to obey the barometer formula, $dP(y)/dy = -\rho(y)g$.

XI. TWO FINITE-RANGE POLYNOMIAL PAIR-POTENTIAL FAMILIES

In our exploratory work here we have emphasized Lennard-Jones' 12/6 pair potential because its thermodynamic properties are familiar and well investigated^{18,19}. Lennard-Jones' potential is the most thoroughly studied of the “realistic” potentials. We have sought to learn more by introducing two very different families of finite-ranged pair potentials. With a triangular lattice the longer-ranged family $\{ \phi_m^L(r < 2) \}$, includes three shells of neighbors, 18 in all, at zero stress, while the short-ranged potentials, $\{ \phi_m^S(r < \sqrt{2}) \}$ include only the six nearest neighbors:

$$\phi_m^L = (2 - r)^{2m} - 2(2 - r)^m \text{ for } r < 2 ; \phi_m^S = (2 - r^2)^{2m} - 2(2 - r^2)^m \text{ for } r < \sqrt{2} .$$

See **Figure 11** for six example plots of these relatively short-ranged potentials. For all of them we will continue to adopt “reduced units” based on a well-depth of unity at the particle-pair separation of unity. All the potentials have smooth minima of -1 at $r = 1$. In the Lennard-Jones case we entirely avoid cutoff corrections by including all $N(N - 1)/2$ pairwise interactions. The finite-ranged polynomial potentials, with order- N interactions, are much faster to analyze. In our exploratory molecular dynamics simulations we enclosed a few hundred particles in a box with quartic-potential very smooth boundaries and included a weak gravitational field. Our plan was to observe phase boundaries directly.

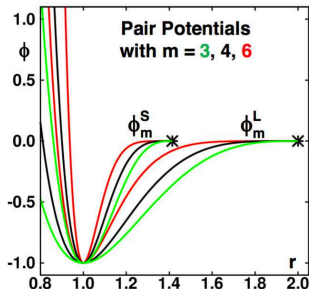


FIG. 11: Two families of pair potentials, $\phi_m^L = (2-r)^{2m} - 2(2-r)^m$ and $\phi_m^S = (2-r^2)^{2m} - 2(2-r^2)^m$. In the stress-free triangular lattice the short-ranged potentials, $\{ \phi_m^S(r < \sqrt{2}) \}$, have a range $\sqrt{2}$ so that each particle only interacts with 6 nearest neighbors. In the longer-ranged case, with $\phi_m^L(r < 2)$, each particle interacts with 3 shells of 6 neighbors each.

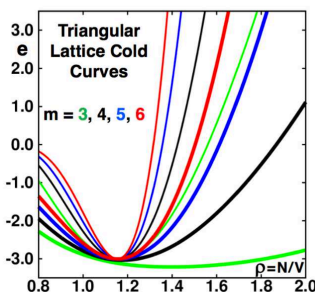


FIG. 12: Cold curves for the triangular lattice with eight potentials of the two types shown in **Figure 11**. The stress-free square lattices are mechanically unstable to shear. The energies with wider bowls are drawn with the wider lines. Those bowls, extending to $r = 2$, include second and third neighbors at zero stress so that the corresponding densities exceed the narrower-bowl value $\sqrt{4/3} = 1.1547$.

The polynomial potentials require simulation times of order N rather than N^2 for the force calculations. **Figures 11 and 12** show six of the specimen potentials along with eight of their static-lattice “cold curves”, calculated for perfect triangular lattices. For the range of densities shown all the shorter-ranged potentials, $\{ \phi_m^S \}$, have their minima at $r = 1$ with cold curve minima at a density $\sqrt{4/3} = 1.1547$ and a binding energy $e(\rho = 1.1547) = -3$. Because the longer-ranged potentials extend to a separation of 2 their lattices are slightly compressed from the “close-packed” density 1.1547. The binding energy is accordingly increased. See **Figure 12**.

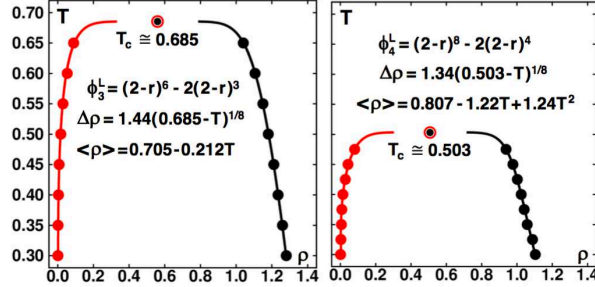


FIG. 13: Coexisting densities for ϕ_3^L and ϕ_4^L . Both cases closely reproduce Onsager’s two-dimensional Ising model power law dependence of the density difference, $\rho_{Liquid} - \rho_{Gas}$ on $T_c - T$. The Mayers’ 1940 “Derby Hat” idea for the region above the meniscus’ disappearance appears in **Figure 14**. Each of the data shown here was generated with a million timesteps using $dt = 0.001$.

XII. GAS LIQUID COEXISTENCE AND THE MAYERS’ “DERBY HAT”

Figure 13 shows our estimates for the gas-liquid coexistence curves for two of the short-ranged potentials. These coexistence curves were obtained using an improved version of the “liquid-ribbon” method described by Farid Abraham in 1980, using 256 particles. Here we use conventional molecular dynamics ($N = 3600$, $dt = 0.001$, $t = 2000$), with a cell, elongated horizontally and with periodic boundaries at its top and bottom. Smooth particle averaging with Leon Lucy’s weight function then provides density and pressure profiles. The initial square-lattice configuration is quenched into the mechanically unstable region of the phase diagram using Nosé-Hoover dynamics. The system rapidly separates into vapour and liquid phases. The density profile is symmetrized prior to recording the values of the flat regions of the gas and liquid phases’ densities. The final configuration of each simulation becomes the starting point for the next-lower temperature simulation. The full set of eight coexisting density pairs is then correlated with their temperatures, as shown in **Figure 13**.

The coexistence data are then fitted to the scaling laws shown in the figure. For the variation of the density with temperature, $\Delta\rho(T)$, the exponents $1/7.5$ and $1/7.9$ resulted for the $6/3$ and $8/4$ long-ranged ($r \leq 2$) potentials, ϕ_3^L and ϕ_4^L . Because these exponents approximate Onsager’s $1/8$, found analytically for the two-dimensional Ising model, we repeated the scaling law fits using $1/8$ for the exponent.

The “Law of Rectilinear Diameters” (the mean of gas and liquid densities varies linearly with temperature) was adequate for the $6/3$ potential while a quadratic fit was needed in the righthand plot of the $8/4$ data. These choices enabled the vapour (red in **Figure 13**)

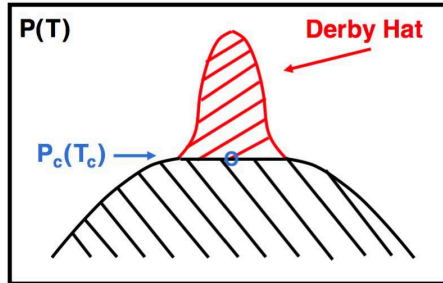


FIG. 14: The Mayers’ 1940 idea, now obsolete, that a meniscus-free region of infinite compressibility (shaped like a “Derby Hat”) would be found atop the two-phase coexistence region, is illustrated here in red. Our simulations carried out above the critical temperature and with a small gravitational field show the presence of relatively large clusters of particles in the low-density upper portions of our containers, as shown in **Figure 15**.

and liquid (black in that figure) densities to be drawn in as continuous curves with critical temperatures of 0.685 and 0.503. We abandoned an effort to estimate the critical region for the 10/5 potential, ϕ_5^L . The relatively weaker binding energy indicated that weeks of computer time might be required for an accurate assessment of that potential’s critical point.

In 1940, as described in Chapter 14 of their *Statistical Mechanics* text²⁰, Joseph and Maria Mayer argued from the standpoint of their statistical-mechanical cluster theory that there is a highly-complex “Derby-Hat” critical region atop the coexistence curve, as is shown in **Figure 14**. The red “Hat” region was thought to sit atop the two-phase region in which gas and liquid are separated by a meniscus. If this construction were correct, as has been recently championed by Woodcock and Khmelinskii²¹, the meniscus should suddenly vanish at the same temperature but at a whole range of different densities, different by as much as ten percent according to the Mayers’ estimate in three space dimensions. Here the main difference seen above and below the apparent critical temperature of 0.685 for the ϕ_3^L potential is the concentration of large clusters in the vapour phase, visible in **Figure 15**.

These polynomial potentials avoid cutoff corrections. We briefly considered the usefulness of energy comparisons with the square lattice, but preliminary calculations revealed that lattice unstable to shears parallel to either the x or the y direction. By contrast, as is consistent with hexagonal symmetry, the triangular lattice has an isotropic shear modulus, a convenient property for modeling atomistic results with isotropic continuum mechanics.

Either type of potential choice, $(2 - r)^{12} - 2(2 - r)^6$ or $(2 - r^2)^6 - 2(2 - r^2)^3$, can provide

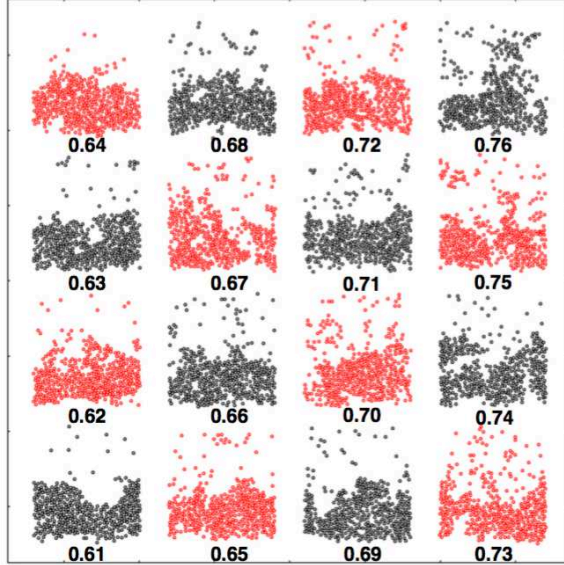


FIG. 15: Sixteen snapshots of 400 particles with $\phi_3^L(r < 2)$ controlled by a gravitational field $g = 0.01$. The periodic width of the system is $\sqrt{800}$. Quartic repulsive potentials, $(1/4)dy^4$, apply beyond the horizontal bounds $|y| = \sqrt{200}$. The spacing between the snapshots is 20,000 timesteps, corresponding to an elapsed time of 100. The lefthand columns, starting at lower left, correspond to subcritical temperatures of 0.61 to 0.68 and the righthand columns to supercritical temperatures from 0.69 to 0.76, finishing at the upper right. The laptop time for all these simulations is a few minutes.

the same curvature at the potential minimum of unity $\phi'' = 72$ as does Lennard-Jones' potential. **Figure 16** shows pressure-density isotherms for all the potentials considered here. The short-ranged potentials' isotherms have a positive compressibility (positive slope in the figure) while Lennard-Jones' and the longer-ranged potentials have negative regions corresponding to the presence of van der Waals' loops and gas-liquid coexistence.

XIII. TIME-AVERAGED THERMOSTATED MOLECULAR DYNAMICS

Figure 15 showed snapshots, equally-spaced in time and in temperature, of 400 longer-ranged ϕ_3^L particles in a gravitational field. The temperature increased stairstep-fashion from 0.61 in the lower left corner to 0.76 at the upper right. There are eight snapshots below the critical temperature and eight above. Although the fluctuations are large it is clear that the cooler subcritical configurations are qualitatively closer to a gas-liquid interface than

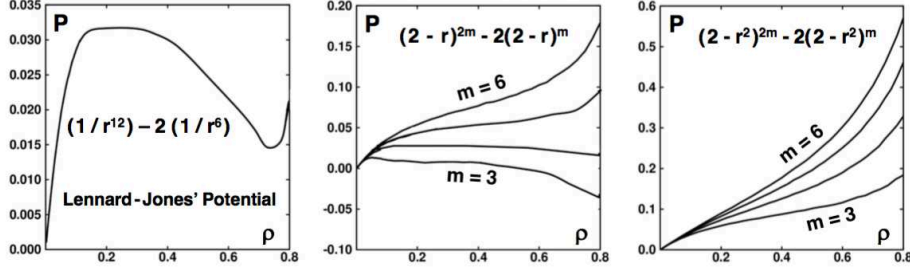


FIG. 16: $T = 0.5$ isotherms for Lennard-Jones' potential and two families of polynomial potentials. The longer-ranged potentials, $\{ \phi_m^L(r < 2) = (2 - r)^{2m} - 2(2 - r)^m \}$, with $m = 3, 4, 5,$ and 6 , appear to exhibit liquid phases while the nearest-neighbor shorter-ranged potentials, $\{ \phi_m^L(r^2 < 2) = (2 - r^2)^{2m} - 2(2 - r^2)^m \}$, appear to go directly from the solid to the gas phase on heating, with no intermediate liquid phase. Approximately 500 simulations were carried out for these isotherms, all with $dt = 0.001$, one million timesteps, and Nosé-Hoover control of the temperature using $\dot{\zeta} = 10[(K_t/K_0) - 1]$. These data have been smoothed slightly for clarity.

the more diffuse supercritical configurations to the right. The fluctuations evident in the snapshots can largely be removed by time averaging. **Figures 17 and 18** show density and pressure profiles with one million timesteps for each temperature. The eight subcritical isotherms show a relatively sharp transition to a lower density gas-phase plateau. Above the critical temperature the density follows the barometer formula with a decreasing density and pressure with altitude. The gravitational field organizes the fluid without noticeably perturbing the structure of the meniscus.

XIV. THE VIRIAL SERIES, DIFFUSION, AND A MOVIE

In working to understand “What is Liquid” we found that gravity and time averaging were useful computational tools. Gravity makes it possible to see an entire isotherm by stabilizing a stationary equilibrium pressure gradient, $(\partial P/\partial y)_T = -\rho(y)g$. Time averaging makes it possible to reduce, and nearly to eliminate, the density and pressure fluctuations which would otherwise obscure the structure of the liquid-gas meniscus. Here we consider briefly the utility of three additional tools, the Mayers' virial series, local values of the short-time anisotropic diffusion, and movies of the meniscus' evolution with relatively strong fields.

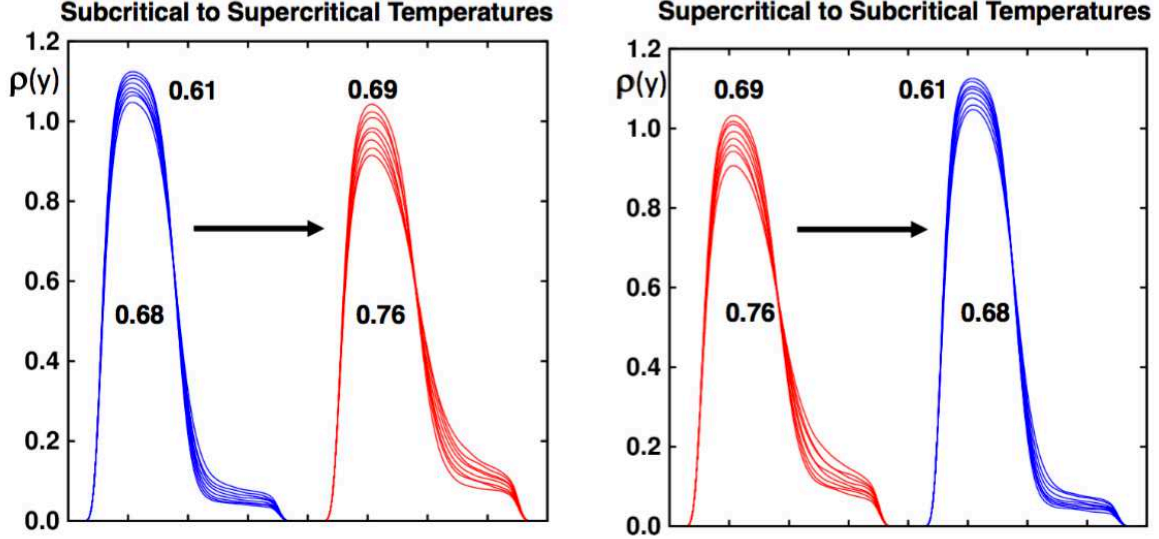


FIG. 17: 16 density profiles, subcritical in blue and supercritical in red, for 16 temperatures ranging from 0.61 to 0.76. The relatively sharp meniscus broadens noticeably at the critical temperature. Each profile is the last-half average of two million Runge-Kutta timesteps with $dt = 0.005$. $N = 400$ in a square container, $L = \sqrt{800}$, periodic at the sides, quartic at the bottom and top, with a gravitational field strength of 0.01. Temperature increases at the left and decreases at the right.

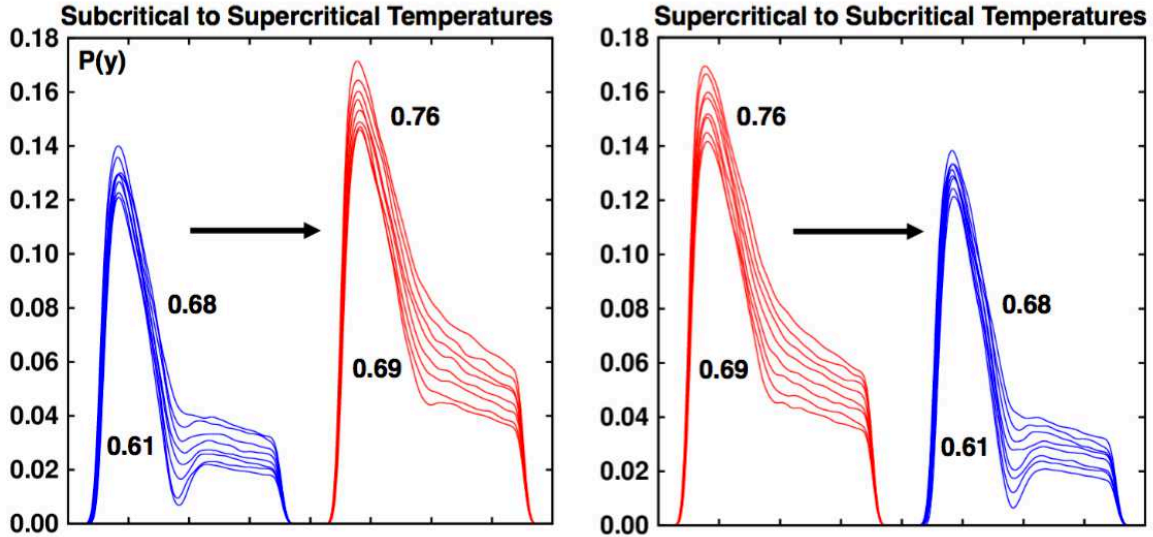


FIG. 18: 16 pressure profiles, subcritical in blue and supercritical in red, for 16 temperatures ranging from 0.61 to 0.76. The dip in the subcritical plots corresponds to the surface tension's negative contribution to the mean pressure, $P = (P_{xx} + P_{yy})/2$. These data, just as those in **Figure 17** required a bit under one day of laptop time. $N = 400$ in a square container, $L = \sqrt{800}$, periodic at the sides, quartic at the bottom and top, with a gravitational field strength of 0.01. Temperature increases at the left and decreases at the right.

A. The Mayers' Virial Series

In principle the Mayers' recipe for the virial coefficients $\{ B_n(T) \}$ provides an exact route to the equation of state by formulating the pressure as a series in the density,

$$PV/NkT = 1 + B_2\rho + B_3\rho^2 + B_4\rho^3 + B_5\rho^4 + \dots .$$

The efficient calculation of the higher coefficients in the Mayers' series has been greatly improved by Richard Wheatley's work²². For hard spheres the fluid equation of state is well known from computer experiments. Wheatley's 12-term series agrees with these experiments within a fraction of a percent, all the way to freezing at $(2/3)$ the close-packed density. Given that success one might well expect that analogous calculations for our polynomial potentials would be useful near the critical point. On the other hand, for ϕ_3^L at the critical point, the unit-distance maximum of the n -body Mayer-function integrands,

$$\prod f_{ij}(r_{ij} = 1) \equiv \prod [e^{1/0.685} - 1] \simeq 3.3^{n^2/3} ,$$

for large n , suggests convergence difficulties for the series. Numerical investigation of the first five terms for $\phi_3^L(r < 2)$ confirms this problem. Monte Carlo evaluation of the Mayer integrals with 10^{11} configurations each gives the following results at the critical temperature, $T_c = 0.685$:

$$\{ B_2 = -4.25589 ; B_3 = -0.176 ; B_4 = 36.7 ; B_5 = 58 \} .$$

Qualitatively the numbers are even less promising for $\phi_4^L(r < 2)$ and for Lennard-Jones' 12/6 potential. Evidently the virial series will not help our understanding. Even with the help of the diminishing powers of the critical density, 0.560^{n-1} , it is clear that the series is poorly behaved. For ϕ_3^L at the critical point we find $PV/NkT = 1 - 2.38 - 0.06 + 6.45 + 6 \dots$, which looks quite hopeless. We conclude that the virial series is not a useful tool in the vicinity of the critical point.

B. Short-Time Diffusion and the Gas-Liquid Transition

As the gas and liquid phases, with their different densities, have correspondingly different diffusion coefficients it is worth investigating the anisotropy of the diffusion induced by the gravitational field's pressure gradient. Away from the meniscus we expect that the

averaged mean-squared displacement will be typical of the field-free displacements,

$$\langle [x(t) - x(0)]^2 \rangle = \langle dx^2 \rangle \simeq \langle [y(t) - y(0)]^2 \rangle = \langle dy^2 \rangle .$$

In the dilute gas limit there is an apparent difference. At time t and in the absence of collisions, the mean-squared x displacement is given by the Maxwell-Boltzmann's mean squared value, $(kT/m)t^2$ while the mean-squared y coordinate, $\langle [\dot{y}(0)t + (g/2)t^2]^2 \rangle = (kT/m)t^2 + (g^2/4)t^4$ is bigger. In the dense solid, on the other hand, both displacements are tiny.

A more formal demonstration of the equilibrium distribution function in a field follows from the Boltzmann equation for the probability density $f(t, y, p)$:

$$(\partial f / \partial t) + p_y (\partial f / \partial y) - g (\partial f / \partial p_y) = \text{collision term} .$$

At low density the two-body collision term can be ignored. In the stationary state $(\partial f / \partial t)$ vanishes. The other two terms cancel when f includes $e^{-p^2/mkT} e^{-mgy/kT}$. All that remains is the solution of a particle in the external field, $y(t) - y(0) = p_y(0)t - (1/2)gt^2$.

Consider two equilibrium systems under the influence of gravitational fields of 0.01 and 0.10, illustrated by the late-time snapshots of **Figure 19**. Notice particularly the difference in the vapour pressures. For two similar systems, but with quartic boundaries, **Figure 20** shows the dependence of the diffusive mean-squared displacement on the sampling time Δ . These systems are held at their critical temperature, $T = 0.685$ subject to the same two field strengths, $g = 0.01$ and 0.10 . The smooth-particle averages of dx^2 and dy^2 with vertical quartic boundaries are based on 300 grid points with a smoothing length $h = 2$. The y coordinate associated with these displacement pairs is the mean value, $(1/2)[y(-\Delta t/2) + y(+\Delta t/2)]$. In **Figure 20** the analysis of particle displacements as a function of the vertical coordinate is carried out with a smoothing length $h = 2$ in a square system, $L = \sqrt{800}$. The corresponding one-dimensional Lucy-function is

$$w(z) = (5/4hL_x)(1 - 6z^2 + 8z^3 - 3z^4) ; z = |y_i - y_g|/2 \text{ for } z < 1 .$$

Lucy's function is used to calculate the ratios $\sum_i w_{ig} dx^2 / \sum_i w_{ig}$ and $\sum_i w_{ig} dy^2 / \sum_i w_{ig}$. Here $w_{ig} \equiv w(|y_i - y_{grid}|)$. It is particularly interesting that the short-time vertical displacement at the larger field is significantly greater than the horizontal, as predicted by simple kinetic theory. An exploration of the details would make a rewarding research project. The state dependence of the short-time diffusion is evidently a useful diagnostic tool.

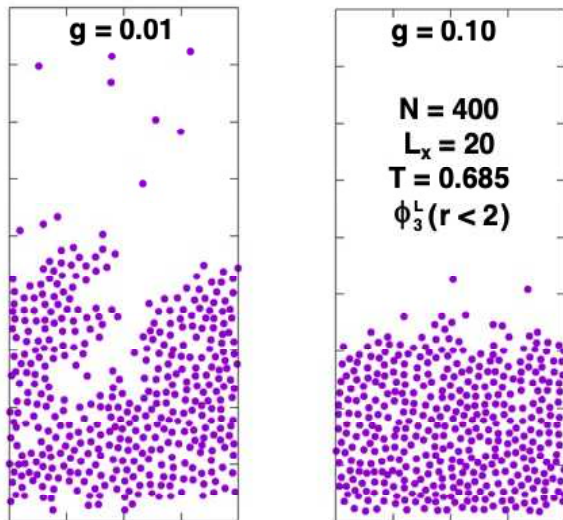


FIG. 19: Typical isothermal equilibrium snapshots of 400 ϕ_3^L particles at the critical temperature 0.685 with gravitational field strengths of 0.01 (at the left) and 0.10 (at the right). Periodic boundaries fix the system width at 20. A quartic boundary at the base supports the weight of the system.

C. Movies of Isothermal Dynamics in a Gravitational Field

In the early days of molecular dynamics computer-generated movies were staples at scientific meetings²³. They showed not only the familiar motion of a gas filling a container, but also the details of shear and heat flows. These movies aided the intuition required to understand atomistic dynamics from the standpoint of continuum mechanics. We expect now that such movies will help lead to understanding the inhomogeneous correlations due to the gradients seen in drops, shockwaves, and gravitational flows. Movies of two-dimensional systems with hundreds or thousands of particles provide valuable insights while requiring very little computer time. A sample movie prepared for the readers of the arXiv and “Computational Methods in Science and Technology”, can be found at the website <http://cmst.eu/wp-content/uploads/2021/03/sim-movie.mp4>. **Figure 21**, taken from a similar movie, shows at the left, the early “spinodal” stage of a 400-particle ϕ_3^L system in

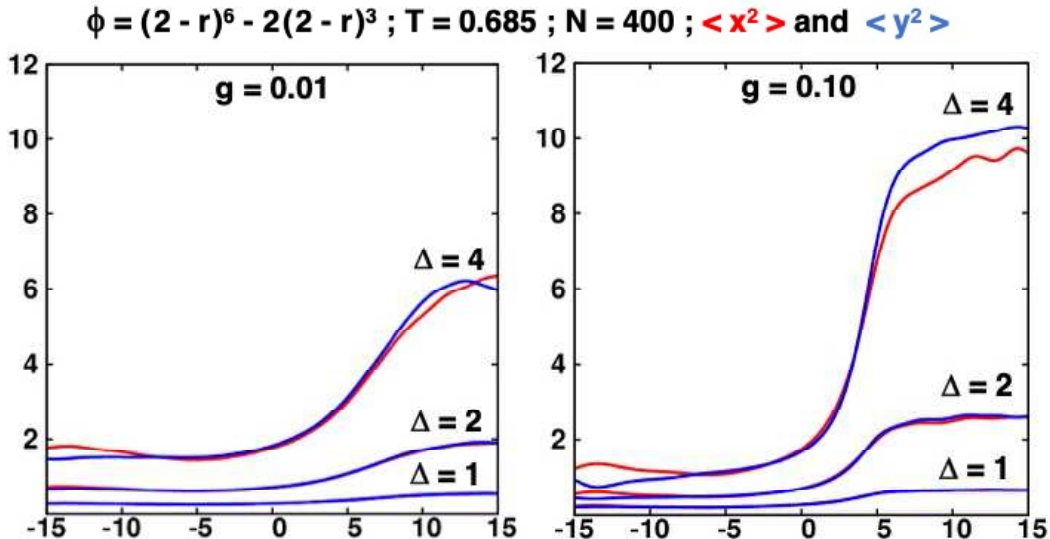


FIG. 20: The mean-squared distances in the horizontal and vertical directions, $\langle x^2 \rangle$ and $\langle y^2 \rangle$ traveled in times Δ of 1, 2, and 4 are plotted as functions of the midpoint y coordinate. The boundary conditions are quartic, in a square box of sidelength $\sqrt{800}$. At the left, corresponding to the weak field $g = 0.01$ there is no significant difference between the mean-squared horizontal and vertical displacements. At the right there *is* a significant difference, with the vertical displacements, shown in blue, larger, as is consistent with collisionless kinetic theory. At the bottom of the container the easier x motion can be seen clearly at the longest time, $\Delta = 4$.

a quartic box with $L = \sqrt{800}$. The gravitational field, in **Figure 21** a relatively large 0.2, supports only a tiny vapour pressure on reaching the equilibrium state shown at the right.

XV. CONCLUDING REMARKS

We have explored the critical region for two varieties of polynomial pair potentials, finding that the shorter-ranged family can sublime directly from the solid phase to the gas, without the intervention of a liquid. The monotone nature of the isotherms of the shorter-ranged potentials, displayed in **Figure 15** is consistent with this finding. The longer-ranged family, with second and third neighbor interactions, form a liquid phase with a well-defined but fluctuating meniscus. Time-averaging the fluctuating profiles provides stable smooth estimates of the meniscus region separating the liquid and gas.

With the longer-ranged potential $(2 - r)^6 - 2(2 - r)^3$ a visual inspection of the heated

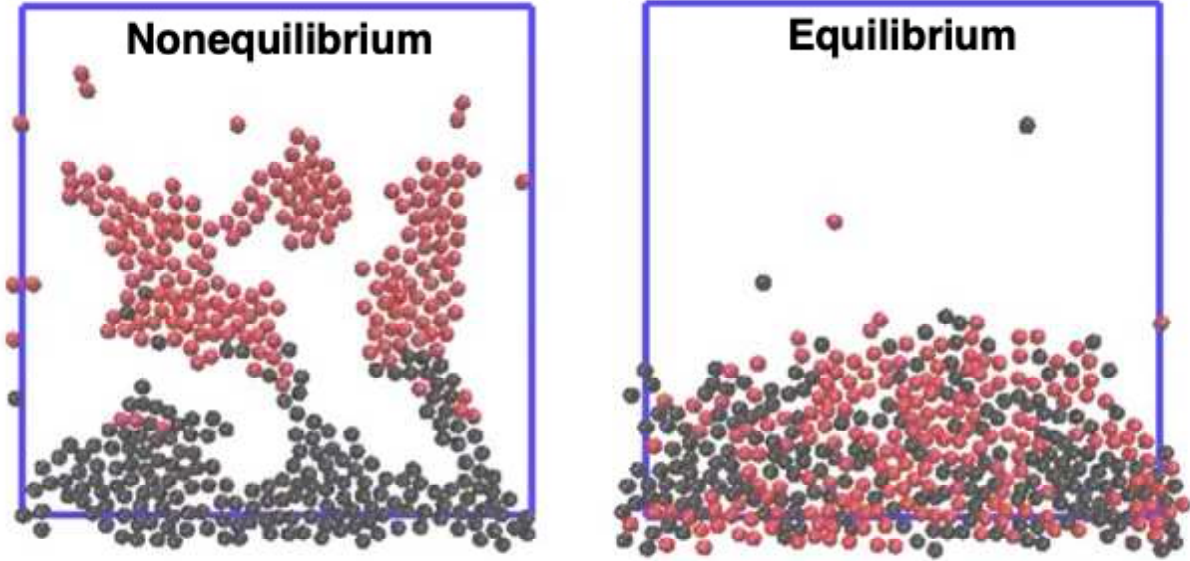


FIG. 21: Two snapshots taken from a computer-generated movie illustrating “spinodal decomposition”, at the left, followed by thermal equilibration under the influence of a “strong” gravitational field, $g = 0.20$. Initially the 400 particles in a square box of area 800 were arranged in an (unstable) square lattice with the upper 200 colored red and the lower 200 black. The pairwise-additive interactions come from the ϕ_3^L potential.

liquid in the presence of a weak field reveals a complexity outside the normal range of thermodynamics. Clusters of particles abound, from dimers and trimers up to percolating clusters which stretch all the way across the simulation. In view of these fluctuating features time-averaging is necessarily required to visualize and stabilize a liquid-gas interface. And time averaging is not enough. In principle field-free time averaging would only produce a constant mean density everywhere!

In order to “see” the definite boundary between liquid and gas we have considered an innovative version of molecular dynamics, with a containerized region and a localizing gravitational field. This combination, when time-averaged, provides density and pressure profiles in which the phases are separated by a meniscus. For small field strengths these profiles resemble the Maxwell construction tie-line linking the two fluid phases below the critical point.

This same technique is equally applicable using Monte Carlo simulations in the canonical ensemble. The presence of gravity provides a definite time-averaged interface, providing a distinction between the gas and liquid and addressing the “What is Liquid” directly, through

Hannay’s interface. The complexities due to fluctuations moderated by surface tension can be overcome with gravity. It is rewarding to see the subcritical dip in the pressure (**Figure 18**) disappear at the estimated critical temperature as calculated independently with an improved version of Abraham’s “liquid-ribbon” technique. It is particularly interesting to see that attractions beyond the first neighbors are needed for the liquid phase.

Jürgen Schnack, in commenting on an earlier draft of this work, pointed out his analogous work (but with a harmonic container) on the molecular dynamics of nuclear matter. In particular that study²⁴ estimated the critical temperature for hot oxygen at 10^{11} kelvins. We also thank John Ramshaw for his cogent remarks on the applicability of hard-sphere perturbation theory to liquid-gas equilibria.

This work achieved two goals. First, we have introduced a useful simulation technique providing a time-averaged description of the liquid-gas meniscus, curved or flat, depending upon the boundary conditions, separating the two phases. Second, we have introduced two families of pair potentials which are relatively short-ranged, thereby avoiding the complications associated with cutoffs. These models have shown that liquids are stabilized by interactions beyond nearest neighbors. Our simulations with gravity generate density gradients spanning a wide range of densities, including the critical density. The method developed here is relatively insensitive to the number of particles chosen and the overall volume of the simulation container. No doubt it will suggest elaborations in conjunction with other stationary processes, both at, and away from, equilibrium.

-
- ¹ Wm. G. Hoover and C. G. Hoover, “Time-Symmetry Breaking in Hamiltonian Mechanics. Part III. A Memoir for Douglas James Henderson [1934-2020]”, *Computational Methods in Science and Technology* **26**, 111-120 (2020).
- ² J. A. Barker and D. Henderson, “What is ‘Liquid’? Understanding the States of Matter”, *Reviews of Modern Physics* **48**, 587-671 (1976).
- ³ Lj. Milanović, H. A. Posch, and Wm. G. Hoover, “What is ‘Liquid’? Understanding the States of Matter”, *Molecular Physics* **95**, 281-287 (1998).
- ⁴ Wm. G. Hoover and C. G. Hoover, “What is Liquid? Lyapunov Instability Reveals Symmetry-Breaking Irreversibility Hidden with Hamilton’s Manybody Equations of Motion”, *Condensed Matter Physics* **18**, 13003:1-13 (2015).
- ⁵ J. A. Barker, D. Henderson, and F. F. Abraham, “Phase Diagram of the Two-Dimensional Lennard-Jones System; Evidence for First-Order Transitions”, *Physica* **106A**, 226-238 (1981).
- ⁶ J. B. Hannay, “The Limit of the Liquid State of Matter”, *Nature*, page 370, 17 August, 1882.
- ⁷ J. S. Rowlinson, “John Adair Barker 1925-1995”, *Historical Records of Australian Science* **11**, 179-190 (1996).
- ⁸ W. W. Wood and J. D. Jacobson, “Preliminary Results from a Recalculation of the Monte Carlo Equation of State of Hard Spheres”, *Journal of Chemical Physics* **27**, 1207-1208 (1957).
- ⁹ B. J. Alder and T. E. Wainwright, “Phase Transition for a Hard Sphere System”, *Journal of Chemical Physics* **27**, 1208-1209 (1957).
- ¹⁰ J. K. Percus and G. J. Yevick, “Analysis of Classical Statistical Mechanics by Means of Collective Coordinates”, *Physical Review* **110**, 1-13 (1958).
- ¹¹ M. S. Wertheim, “Exact Solution of the Percus-Yevick Integral Equation for Hard Spheres”, *Physical Review Letters* **10**, 321-323 (1963).
- ¹² N. Shamsundar and John H. Lienhard, “Equations of State and Spinodal Lines”, *Nuclear Engineering and Design* **141**, 269-287 (1993).
- ¹³ J. Wedekind, G. Chkonia, J. Wölk, R. Strey, and D. Reguera, “Crossover from Nucleation to Spinodal Decomposition in a Condensing Vapour”, *Journal of Chemical Physics* **131**, 114506 (2009).
- ¹⁴ S. W. Koch, R. C. Desai, and F. F. Abraham, “Dynamics of Phase Separation in Two-

- Dimensional Fluids: Spinodal Decomposition”, *Physical Review A* **27**, 2152-2167 (1983).
- ¹⁵ F. Trudu, D. Donadio, and M. Parrinello, “Freezing of a Lennard-Jones Fluid: From Nucleation to Spinodal Regime”, *Physical Review Letters* **97**, 105701 (2006).
- ¹⁶ A. J. C. Ladd and L. V. Woodcock, “Triple-Point Coexistence Properties of the Lennard-Jones System”, *Chemical Physics Letters* **51**, 155-159 (1977).
- ¹⁷ D. Badde, J. Danziger, R. Hook, and J. Walsh, “Leon B. Lucy, 1938-2018”, *The Messenger* **173**, 58-59 (2018).
- ¹⁸ J. A. Blink and Wm. G. Hoover, “Fragmentation of Suddenly Heated Liquids” *Physical Review A* **32**, 1027-1035 (1985).
- ¹⁹ B. L. Holian and D. E. Grady, “Fragmentation by Molecular Dynamics: The Microscopic ‘Big Bang’ ”, *Physical Review Letters*, **60**, 1355-1358 (1988).
- ²⁰ J. E. Mayer and M. G. Mayer, *Statistical Mechanics*, First Edition (John Wiley & Sons, New York, 1940).
- ²¹ I. Khmelinskii and L. V. Woodcock, “Supercritical Fluid Gaseous and Liquid States: A Review of Experimental Results”, *Entropy* **22**, 437, (2020). 26 pages.
- ²² R. J. Wheatley, “Calculation of High-Order Virial Coefficients with Applications to Hard and Soft Spheres”, *Physical Review Letters* **110**, 200601 (2013).
- ²³ B. L. Holian, “Atomistic Computer Simulations of Shockwaves”, *Shockwaves* **5**, 149-157 (1995).
- ²⁴ J. Schnack and H. Feldmeier, “The Nuclear Liquid-Gas Phase Transition Within Fermionic Molecular Dynamics”, *Physics Letters B*, **409**, 6-10 (1977).